RESEARCH ARTICLE

Key Points:
- Valley networks are Hesperian/ Noachian in age
- A global climate supported valley networks
- Fluvial degradation may be related to elevation

Correspondence to:
R. A. Craddock,
craddockb@si.edu

Age dates of valley network drainage basins and subbasins within Sabae and Arabia Terrae, Mars

Sylvain Bouley[1] and Robert A. Craddock[2]

[1]GEOPS (Géosciences Paris Sud), UMR 8148, Orsay, France, [2]Center for Earth and Planetary Studies, National Air and Space Museum, Smithsonian Institution, Washington, District of Columbia, USA

Abstract The precise timing of valley network drainage basin formation is critical to understanding the history of water and climate on Mars. To determine whether there are any variations in ages within separate drainage basins and subbasins that may reflect local or regional variations in climate or resetting from resurfacing (e.g., impact ejecta or lava flows), we dated 27 basins and subbasins in Sabaea and Arabia Terrae. The age-dating basin technique we employed allowed sufficient precision to give accurate ages and shows that fluvial activity within the basins and subbasins ceased at approximately the same time around the Early Hesperian/Late Hesperian transition. Our results support the hypothesis that valley networks formed during a unique "fluvial optimum" that may have shut off gradually because of a global climate change that affected all areas simultaneously on Mars.

1. Introduction

Martian valley networks, which are located primarily in the heavily cratered terrain on Mars [e.g. *Milton*, 1973; *Carr*, 1996], are the best evidence that liquid water may have been stable on the surface at one time and that the past climate may have been warmer than today [*Gulick*, 2001; *Craddock and Howard*, 2002]. Because they are located primarily in Noachian age terrain ($>$3.7 Ga) the general assumption has been that they formed sometime during the end of the Noachian Period and possibly through the beginning of the Hesperian Period [*Tanaka*, 1986; *Scott and Tanaka*, 1986; *Greeley and Guest*, 1987; *Carr*, 1996; *Hartmann and Neukum*, 2001; *Irwin et al.*, 2005; *Fassett and Head*, 2008; *Hoke and Hynek*, 2009; *Hynek et al.*, 2010; *Hoke et al.*, 2011]. The control of watershed length by earlier Noachian topographic features, which was not significantly modified by relict networks, suggests that the Early to Middle Noachian geomorphic environment was nominally much drier than the later Noachian to Hesperian transition [*Hynek et al.*, 2010; *Irwin et al.*, 2011]. Some studies suggest that limited valley network formation and localized fluvial activity extended into the Late Hesperian [*Mangold et al.*, 2004; *Quantin et al.*, 2005; *Ansan and Mangold*, 2006; *Bouley et al.*, 2009, 2010; *Hynek et al.*, 2010; *Mangold*, 2011]. These observations leave us with many profound questions. Did valley network formation occur simultaneously on a global scale? Were there local or regional variations in the timing of valley network formation? How long did valley network formation last? Did some valley networks remain active longer than others? Is it also possible that impact cratering or local volcanism resurfaced the surrounding landscape and thus frustrated valley network development [*Irwin and Howard*, 2002; *Howard*, 2007]?

One of the obvious problems with age-dating valley networks is the fact that they are small, linear features that are easily destroyed by large impact craters or other processes such as volcanic resurfacing or aeolian air fall deposits; thus, counting craters on valley networks themselves is difficult at best. One approach introduced by *Tanaka* [1982] for age-dating valley network is often referred to as the "buffered crater counting technique" [*Fassett and Head*, 2008; *Hoke and Hynek*, 2009]. In this technique an area or "buffer" 1.5 times the impact crater diameter is established around the edges of a valley network. Craters that are counted include both those having their centers in the buffer and those intersecting the valley segment. With this technique, *Fassett and Head* [2008] dated 26 valley networks in the upland cratered terrains and observed an age variability between 3.5 and 3.81 Gyr (with considerable uncertainty). Hoke and Hynek found a similar age variability (between 3.58 and 3.79 Gyr) for 10 valley networks located in Terra Sabae, Arabia Terra, and Meridiani Planum.

For our study, we adopted an alternative age-dating approach that we refer to as the "basin technique," which is a more traditional method usually used for regional studies but which has been applied to characterize the temporal activity of a given valley network [*Ansan and Mangold*, 2006; *Bouley et al.*, 2010]. Valley networks are contained within drainage basins (or watersheds), which are defined as the area that contributes water to a particular channel or set of channels and is usually delineated by topographic divides [*Leopold et al.*, 1992]. The basin technique consists of counting craters within the whole valley network drainage basin and typically provides the maximum age of the valley [*Bouley et al.*, 2010]. In general, the basin technique provides greater statistical reliability because of a larger number of craters as well as the larger counting area with the tacit assumption that fresh craters contained in the drainage basin record the cessation of fluvial activity. Here we apply this technique on 27 basins and subbasins located in Sabae and Arabia Terrae studied by *Irwin et al.* [2011] because these regions contain some of the most extensive and densest valley networks on Mars. Our analyses help to (1) establish when fluvial processes responsible for valley network formation ceased on Mars, (2) evaluate possible spatial and temporal variability of fluvial processes within a large region on Mars, and (3) assess which age-dating techniques are the most appropriate to understanding temporal variability in valley network formation.

2. Data and Methodology

In support of our analyses, we used Thermal Emission Imaging System daytime thermal infrared images with a spatial resolution of 100 m/pixel [*Christensen et al.*, 2003]. A digital elevation model (DEM) with 1/128 pixel per degree gridded Mars Orbiter Laser Altimeter (MOLA) [*Smith et al.*, 1999] data provided the basis for extracting the 27 basins and subbasins drainage divides as described below. All data were orthorectified to the standard Martian aeroid with an axis of 3396 km using a sinusoidal projection centered at different meridians depending of the basin longitude. We used five different meridians to cover the 50° longitude of the studied region (10 to 50°E). The MOLA DEM has a spatial resolution of ~460 m/pixel and a vertical accuracy of ~1 m.

A variety of algorithms have been written to extract watershed information from gridded elevation data (DEMs) [*Palacios-Velez and Cuevas-Renaud*, 1986; *Martz and Garbrecht*, 1992; *Zhang and Montgomery*, 1994; *Tarboton*, 1997]. Although called by a variety of names, most algorithms are based on the D8 flow model, which determines the flow direction from every grid cell in a DEM by calculating the steepest downhill slope from a grid cell to the eight surrounding grid cells. Cells with undefined flow directions are resolved iteratively by assigning them the lowest values from one of the neighboring cells with defined flow directions. The results are stored as a grid file with the same dimensions as the DEM. The values recorded in each grid cell are representative of the flow direction from that particular cell (e.g., 1 is NE, 2 is E, 4 is SE, and so on).

As the flow path is traced from one grid cell to the next it eventually encounters the flow path from adjacent grid cells. These separable flow paths represent unbranched tributaries referred to as first-order streams. That nomenclature is universally accepted, but there are three different methods of ordering streams after they have joined. *Horton*'s [1945] original method assigns an order for each stream based on its relative importance in the network while *Strahler*'s [1952] method assigns an order to each segment. Strahler's system is less cumbersome in that two first-order streams come together to form a second-order stream, two second-order streams join to form a third-order stream, and so on. Shreve Magnitude [*Shreve*, 1967] assigns an order to each segment based on the number of upstream links formed by tributaries. Most commercial software packages available for drainage basin analyses allow the user to move back and forth between these different systems. Doing so does not change the position of any of the defined channels only what it is called. For simplicity we have used the Horton stream ordering system for our analyses. The subbasins presented in our analyses are all defined by fifth-order streams.

The total area flowing into each cell is defined as the contributing area, and by adding these values for every cell along the flow path of a particular stream, it is possible to calculate the drainage area for that stream. Because such drainage areas fit into the larger drainage basin, they are commonly referred to as subbasins and are denoted by the largest-order stream that they support. By integrating the contributing areas for the entire network, it is possible to determine the surface area for the drainage basin as well as its boundaries or drainage divides. Versions of the D8 flow model are commercially available in several software packages,
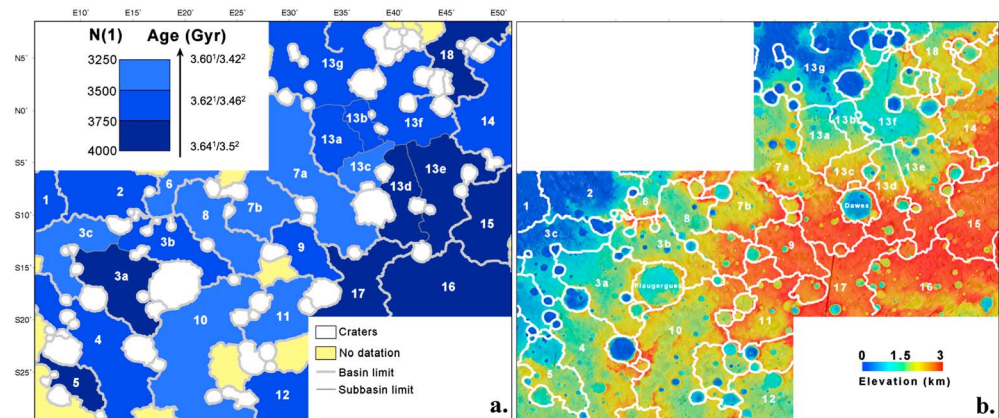
Figure 1. (a) Variation of crater density N(1) (number of craters greater than or equal to $1\,km/10^6\,km^2$) and corresponding N(1) ages (age[1] from *Ivanov* [2001] and age[2] from *Hartmann* [2005]) inside 27 basins and subbasins of Parana Valles subbasin. Details of crater density are given for each number of basin and subbasin in Table 1. Crater density was determined by the basin dating technique. (b) MOLA topographic map of the Sabae and Arabia Terra region with the delineated drainage divides of the 27 studied basins and subbasins.

including RIVIX's RiverTools and Environmental Systems Research Institute's ArcInfo. Both programs provide a variety of automated analyses, such as calculation of the relief and average elevation of the entire drainage basin as well as the individual subbasins. Both programs can also account for the shape of the Martian aeroid; thus, relevant measurements are made accurately. In addition, both RiverTools and ArcInfo allow results to be saved as vector files that can be analyzed in other geographic information system programs. Stream order is also assigned to each valley network automatically. In fact, a number of planetary investigators have used the D8 algorithm to analyze MOLA data in support of similar analyses [*Banerdt and Vidal*, 2001; *Mest and Crown*, 2001; *Aharonson et al.*, 2002; *Irwin et al.*, 2002; *Stepinski et al.*, 2002].

The basins and subbasins drainage divides delineated in our analyses were also mapped previously by *Irwin et al.* [2011]. Similar to *Irwin et al.* [2011], we removed the effects of post-Noachian landforms such as fresh impact craters and delineated drainage divides from the MOLA topography (Figure 1b). We age dated basins W1 to W17 and subdivided the largest watersheds (W3,W7, and W13) into subbasins based on the location of valley network tributaries and topographic divide.

We counted craters with diameter of 1 km and larger inside the 27 different basins and subbasins. For each drainage basin, we counted craters only where the contributing area was obviously related to the watershed. We also excluded areas where there were young depositional surfaces (e.g., crater basin interiors); however, such surfaces were usually topographically separable from the drainage basins or could be clearly mapped. As indicated on Table 1, the surfaces we used for counting craters represent 20 to 100% of the total basin areas.

Because of statistical errors and possibility of overinterpreting too much from any one crater size, we measured craters at N(1), N(2), and N(5) values. N(1) ages are most useful for dating some of the smaller drainage basins, and because smaller diameter craters occur in greater numbers, they tend to offer a statistically more reliable sampling. However, they are also the most susceptible to eradication by processes that occurred after the cessation of fluvial processes (e.g., aeolian modification) and by contamination by secondary impacts. Obviously, if a ~1 km diameter crater had been eradicated from the local population following valley network formation processes, we could not tell, which is why larger diameter craters also need to be considered. However, the tacit assumption we make is that our populations are fully preserved and reflect the ages of the surfaces following valley network formation.

Secondary impact craters are also another source of concern when evaluating crater populations. For example, *McEwen et al.* [2005] suggested that 75% of the craters superimposed on the floor of Athabasca Valles are secondary craters and cautioned that this affects the interpretation of ages. In the case of Athabasca Valles, it was particularly important to evaluate the influence of secondary impact craters because the lava plains in this region are very young (<100 Ma) and contain very few craters to begin with. In our

Table 1. N(1), N(2), and N(5) and Uncertainties Calculated for the 27 Basins and Subbasins Using Basin Dating Technique[a]

		Basin Sup.	Count Sup.	Count N(1)	N(1)	±	N(1) Age(1)	N(1) Age(2)	±	Count N(2)	N(2)	±	Count N(5)	N(5)	±
1		58441	40915	153	3743	302	3,63	3.49	0.03	40	978	155	17	415	101
2		129964	79135	290	3667	215	3.63	3.48	0.02	84	1061	116	21	265	58
3	a	137110	134153	496	3698	166	3.63	3.48	0.01	118	880	81	27	201	39
	b	108523	60429	236	3908	254	3.64	3.5	0.02	64	1059	132	9	149	50
	c	109347	67145	228	3397	225	3.61	3.44	0.02	56	834	111	10	149	47
4		206995	72644	261	3595	222	3.62	3.46	0.02	49	675	96	9	124	41
5		49644	49553	193	3898	280	3.64	3.5	0.03	38	767	124	9	182	61
6		56844	56405	184	3264	241	3.6	3.43	0.02	52	922	128	13	230	64
7	a	256401	90916	307	3379	193	3.61	3.44	0.02	77	847	97	18	198	47
	b	99982	67442	232	3442	226	3.61	3.44	0.02	67	993	121	17	252	61
8		125013	58244	198	3392	241	3.61	3.44	0.02	44	755	114	9	155	52
9		72851	15798	56	3515	472	3.61	3.44	0.03	13	823	228	3	190	110
10		277982	79002	257	3255	203	3.6	3.43	0.02	67	848	104	16	203	51
11		90279	59892	195	3251	233	3.6	3.43	0.02	41	685	107	10	167	53
12		83510	20700	74	3552	414	3.62	3.46	0.03	21	1014	221	6	290	118
13	a	82708	77252	272	3523	214	3.62	3.46	0.02	66	854	105	17	220	53
	b	41182	37214	131	3510	307	3.61	3.45	0.03	45	1209	180	6	161	66
	c	47775	47180	161	3416	269	3.61	3.45	0.02	33	699	122	7	148	56
	d	88627	79229	299	3768	218	3.63	3.49	0.02	75	947	109	12	151	44
	e	162761	146463	570	3891	163	3.64	3.5	0.02	128	874	77	30	205	37
	f	158357	57792	210	3634	251	3.62	3.47	0.02	60	1038	134	7	121	46
	g	183320	89965	317	3526	198	3.61	3.45	0.02	81	900	100	24	267	54
14		171517	45389	163	3598	282	3.62	3.46	0.03	34	749	128	10	220	70
15		129752	48201	186	3849	283	3.64	3.49	0.02	42	871	134	8	166	59
16		243274	72143	271	3757	228	3.63	3.48	0.02	54	749	102	12	166	48
17		121407	25677	98	3802	385	3.63	3.48	0.03	15	584	151	0	0	0
18		102961	70981	269	3792	231	3.63	3.48	0.02	83	1169	128	12	169	49
Total		3396529	1749858	6306	3598	45	3.62	3.4637037037037	0.02	1547	884	22	339	194	11

[a]The basin and subbasin numbers correspond to those presented in Figure 1. The basin area is the area of the basin defined by *Irwin et al.* [2011]. The count area is the surface area used to determine the N(1), N(2), and N(5) crater populations. Count N(1), N(2), and N(5) are respectively the number of counted craters larger than 1 km, 2 km, and 5 km. N(1) age[1] and N(1) age[2] are respectively calculated from *Ivanov* [2001] and *Hartmann* [2005] Martian chronology functions.

study, however, the Hesperian and/or Noachian terrains included a greater number of craters, so the amount of contamination by secondaries is smaller by comparison. In addition, we avoided the potential effects of secondary impact craters by purposely excluding regions where there were abnormally high small crater concentrations, which are often indicative of secondaries. The presence of secondary craters in the counting regions is still possible, particularly at smaller diameters of ≤1 km, but we assume they would not affect the age-dating results because they likely represent a small percentage of the total observed craters.

The resulting densities of D ≥ 1 km, 2 km, and 5 km craters were normalized to an area of 10^6 km^2 to determine the formation period of the valleys using established crater density boundaries [*Tanaka*, 1986; *Ivanov*, 2001; *Tanaka et al.*, 2005; *Hartmann*, 2005; *Werner and Tanaka*, 2011]. Uncertainties represent a 1σ interval of $\pm \sqrt{N(X)}/A$ with N(X) the number of craters of more than X km and A the basin area. As a basis for easy comparison, we calculated an absolute age (T in Gyr) for each basin and subbasin using N(1) and the Martian chronology functions:

$$N(1) = 2.68 \times 10^{-14}(\exp(6.93T) - 1) + 4 \times 13.10^{-4}T \quad (1)$$

[*Ivanov*, 2001]

$$N(1) = 4.42 \times 10^{-14}(\exp(6.93T) - 1) + 6 \times 82.10^{-4}T \quad (2)$$

[*Hartmann*, 2005]

Because of the large uncertainties in applying absolute ages to Martian surfaces [*Hartmann and Neukum*, 2001], it should be cautioned once again that these ages may be imprecise and are thus more useful to qualify (as opposed to quantify) the variability in different basins ages.

We also plotted incremental crater densities using a modified Hartmann diagram [*Hartmann*, 2005]. The Hartmann diagram gives a complete display of the relationship between crater density and diameter. In

order to compare basin ages during Noachian and Hesperian periods, we normalized the crater density from the Early/Late Hesperian isochron. In ordinate, the value is without dimension and is equal to $N(X)/N(X)_{EH/LH}$ where $N(X)$ is the crater density for a X km diameter class and $N(X)_{EH/LH}$ the crater density of the Early/Late Hesperian isochron for a X km diameter class. The Early/Late Hesperian (3.4 Gyr) and the Noachian/Hesperian (3.54 Gyr) isochron ordinates are equal to 1 and 1.6, respectively [*Hartmann*, 2005].

3. Age-Dating Drainage Basins

3.1. Study Areas

We dated 27 basins and subbasins in three highland study areas defined by *Irwin et al.* [2011]. The three study areas included Sabae West (5–32°E, 5–30°S), Sabae East (0–20°S, 32–52°E), and Arabia Terrae (0–10°N, 28–53°E). These three regions are located in the northwestern part of Hellas basin between 0 and 3000 m elevation (Figure 1b). The flow direction within the valley networks was mainly toward the north, northwest, and west (W1 to 9, W13 to 15, and W18). W10 is drained toward a large graben (flow to SW), W11 and W12 are endorheic basins (flow to east), and W16 and W17 are Hellas-oriented networks that drain toward the southeast. Many of the drainage basins related to shorter valley networks are also endorheic and are controlled by the topography associated with large, degraded impact basins, including Flaugergues, Dawes, Schiaparelli, and Huygens. Five of the drainage basins we studied are open and are drained by valley networks that follow long regional slopes (Mosa/Evros Valles (W3), Marikh Vallis (W4), Verde Vallis (W7) and Naktong Vallis (W13), and Locras Valles (W18)).

3.2. N(1), N(2), N(5), and Basin Age Variability

Sabae and Arabia Terras were divided into 27 basins and subbasins. The three largest basins W3, 7, and 13 were subdivided into 3, 2, and 7 subbasins, respectively. The surface areas range from 41,182 km^2 (W13b) to 277,982 km^2 (W10). In each basin or subbasin, we measured N(1), N(2), and N(5) with 1σ errors (Table 1) with contributing areas ranging from 15,798 km^2 (W9) to 146,464 km^2 (W13e). In total, we counted 6306 craters with an area of 1.74×10^6 km^2.

The plots of N(1), N(2), and N(5) crater densities are presented in three different diagrams (Figure 2), which allows us to compare the values and corresponding ages between each basin. As shown in Figure 2, the N(1), N(2), and N(5) crater densities in the different basins and subbasins are not homogeneous. Specifically,

1. We distinguished three different groups of N(1) ages. Eight different basins have N(1) age values ranging from 3250 to 3500, 10 others have N(1) value ranging from 3500 to 3750, and eight others ranging from 3750 to 4000. The difference of N(1) craters between basins can be as great as 650. Table 1 shows that most of N(1) error bars range between 200 and 400, suggesting that the N(1) variability is statistically separable and may reflect differences in geologic history. It should also be noted that despite this variability, N(1) and the studied basins are all the Early Hesperian/Late Hesperian in age according to plots by *Tanaka* [1986] and *Hartmann* [2005]. On the *Ivanov* [2001] plot they are younger than the Early Hesperian boundary.

2. N(2) and N(5) ages have much greater variability than those calculated for N(1) (Figure 2). While the N(1) ages for the studied basins are all within the Early Hesperian/Late Hesperian (EH/LH) range, the N(2) ages range from values of 600 (Early Hesperian/Late Hesperian-EH/LH) to 1200 (Nochian/Early Hesperian-N/EH). N(5) ages also range from 100 (Early Hesperian/Late Hesperian-EH/LH) to 400, which is well into the Noachian (N).

The N(2) and N(5) ages have a large variability because the number of craters decreases significantly at increasing diameters. In each basin, we counted an average of 234 craters with D ≥ 1 km, 56 craters with D ≥ 2 km, and 13 craters with D ≥ 5 km. The sampling is 4 times larger between N(1) and N(2) and 20 times between N(1) and N(5). Recalling the caveats when considering the N(1) ages, the problem now is that the smaller N(2) and N(5) sampling sizes make their ages less reliable. For these reasons, when evaluating the age variability between basins and subbasins and determining when fluvial processes ceased, it is important to include analyses of N(1), N(2), and N(5) crater populations.

From the Ivanov equation (1) and Hartmann equation (2), we calculated N(1) ages for the subbasins to assess any potential variability in the absolute ages (Table 1). An N(1) range from 3250 to 4000 corresponds to a small N(1) age range from 3.6 to 3.64 Gyr (beginning of Late Hesperian for *Ivanov* [2001]) and from 3.43 to
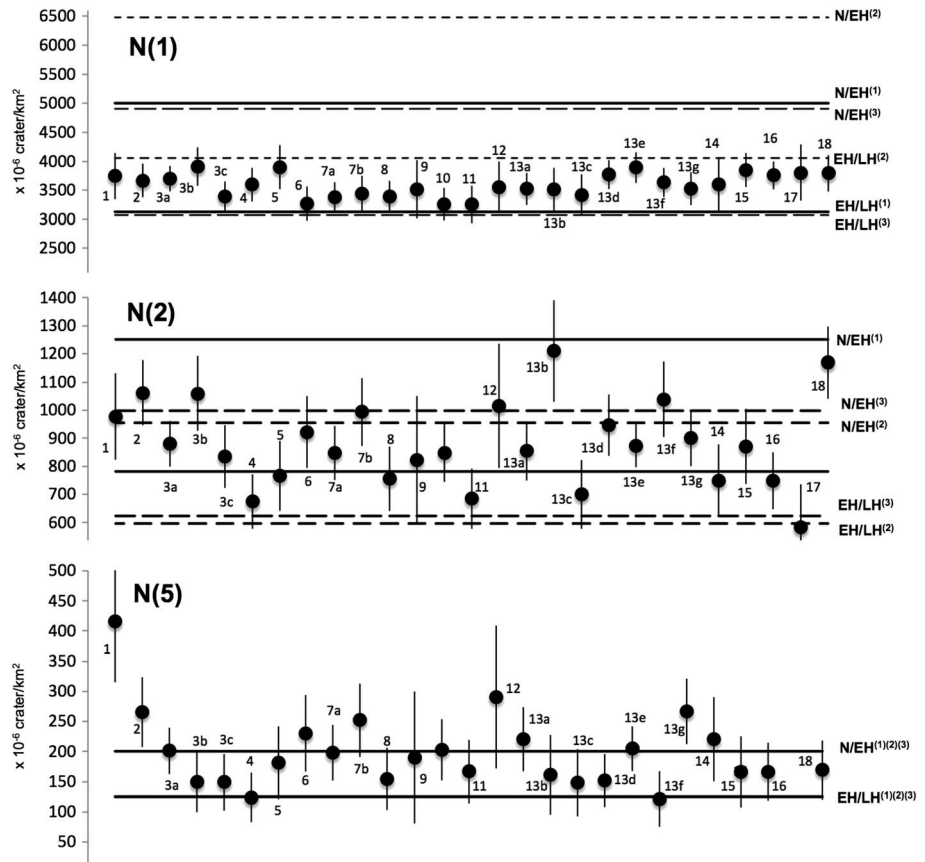
Figure 2. N(1), N(2), and N(5) with error bars given for each number of basin and subbasin in Table 1. N/EH boundary represents the Noachian/Early Hesperian boundary, and EH/LH represents the Early Hesperian/Late Hesperian boundary. For the N(1), N(2), and N(5) boundaries, different size-frequency distribution shapes were used: (1) a minus-two-slope power law and values from *Tanaka* [1986], *Tanaka et al.* [2005], and *Werner and Tanaka* [2011], (2) the description by *Ivanov* [2001], and (3) a cumulative version of the description by *Hartmann* [2005].

3.5 Gyr (end of Early Hesperian for *Hartmann* [2005]). Because of the large uncertainties in applying absolute ages to Martian surfaces, the variability of the N(1) age around the 3.62 Gyr [*Ivanov*, 2001] and 3.46 Gyr [*Hartmann*, 2005] values observed on Figure 3 and the average N(1) age uncertainties of 0.02 [*Ivanov*, 2001] and 0.03 [*Hartmann*, 2005] Gyr calculated in Table 1 indicate that the perceived age variability is not completely convincing. Nevertheless, as we suggested previously, this small variability may be correlated to geological history.

Assuming first that fluvial activity ceased simultaneously on the different watersheds, the cause of the observed (albeit subtle) N(1) variability needs to be explained. We plotted crater densities of the three different N(1) value groups [3250–3500], [3500–3750], and [3750–4000] on a modified Hartmann diagram
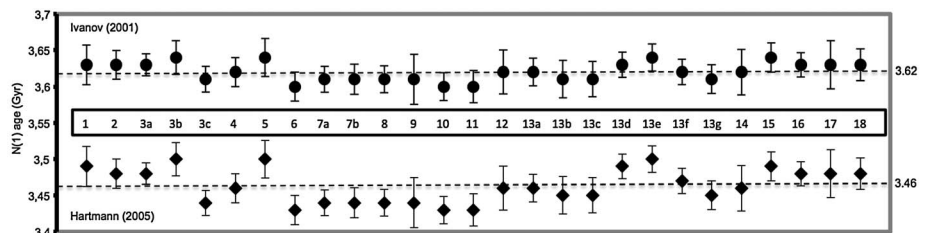
Figure 3. N(1) age with error bars given for each number of basin and subbasin in Table 1. The age is derived from the chronology model of *Ivanov* [2001] and *Hartmann* [2005].
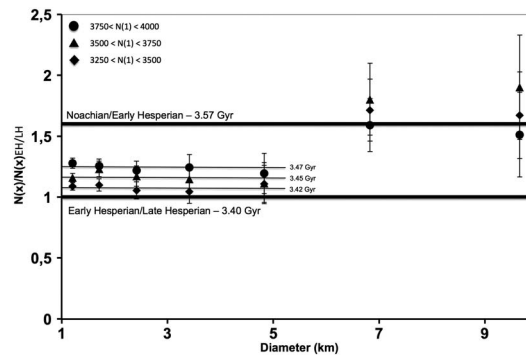
Figure 4. Incremental crater densities of the three N(1) basin groups [3250–3500], [3500–3750], and [3750–4000] on the *Hartmann* [2005] modified diagram. Crater densities are normalized from the Early/Late Hesperian isochron. The Early/Late Hesperian (3.4 Gyr) and the Noachian/Hesperian (3.56 Gyr) isochron ordinates are respectively equal to 1 and 1.6. The boundaries ages are derived from *Hartmann* [2005].

(Figure 4) to see if the N(1) variability could be the result of a resurfacing event (i.e., a preservation effect). Analysis of Figure 4 suggests that the three basin groupings are the result of a resurfacing event that created a deficit of craters < 7 km in diameter. The population densities for craters >7 km in diameter give a Late Noachian/Early Hesperian age for the drainage basins, while craters <7 km in diameter give a variable Early Hesperian age ranging from 3.42 to 3.47 Gyr. The age range calculated by this method is also small and indicates very similar ages. The age for each group is consistent with N(1) values giving a younger age for the [3250–3500] group and an older age for the [3750–4000] group (Figure 4 for D ≤ 5 km).

3.3. Possible Origin of the N(1) Spatial Variability

We compared the N(1) spatial variability to the topography to understand why there is a small difference of 1–7 km crater densities between the three different N(1) groups. As observed in Figure 1, basins with high N(1) values [3750–4000] are located primarily in southeast of Sabae Terra (W13d and W13e, W15 to W17), east of Arabia Terra (W18), and west of Flaugergues craters (W3a). All these basins are located at either the highest elevations in this region between 2000 and 3000 m (W13d and e, W15 to 18) or—importantly—represent the upstream subbasins of the largest drainage basins (W3 and W13). Downstream subbasins (W3c, 13g, and 13f) of the two larger basins have smaller N(1) values ranging from 3250 to 3750. It is more difficult to see an obvious relationship for the other basins except that they are typically located at an elevation between 0 and 2 km. Our results suggest that the deficit of 1–7 km crater in diameter is smaller for higher-elevation terrains. This conclusion should be taken carefully because of the uncertainties of N(1) determination. Nevertheless, this observation could be consistent with some other studies that suggested fluvial processes were not as intense at higher elevations and waned gradually as a function of elevation [*Scott and Dohm*, 1992; *Craddock and Maxwell*, 1993; *Bouley et al.*, 2010; *Irwin et al.*, 2013]. Thus, our interpretation is that the paucity of craters at lower elevations may reflect the continuation of fluvial processes at lower elevations, which would imply a nonsynchronicity of termination of valley network formation. If the depletion of smaller diameter craters was due to volcanism or aeolian aggradation, then it is more likely that this material would collect at lower elevations [*Irwin et al.*, 2013]. However, we observed no evidence of volcanic flows or ash and dust deposits within any of the basins we investigated. Again, the principal conclusion we reach is that the crater populations suggest that there was more intense/prolonged fluvial erosion at lower elevations.

4. Discussion

4.1. Drainage Basin Ages

Our assessment of basin and subbasin age dates suggest that fluvial activity ceased simultaneously around the Early Hesperian/Late Hesperian transition (~3.46 Gyr: *Hartmann* [2005] or ~3.62 Gyr: *Ivanov* [2001]) and that only post-Noachian fluvial activity is preserved in Sabae and Arabia Terrae. Cessation of fluvial activity and valley network formation at about the early Hesperian is consistent with interpretations by many other investigators, including *Mangold et al.* [2004], *Quantin et al.* [2005], *Howard et al.* [2005], *Ansan and Mangold* [2006], *Bouley et al.* [2009, 2010], and *Mangold* [2011]. *Fassett and Head* [2008] and *Hoke and Hynek* [2009] determined that the ages of valley network systems within the cratered highlands are Early Hesperian, but they showed a larger age variability that ranges from the Late Noachian to the Early Hesperian. When compared to other regions in the southern cratered highlands [*Carr*, 1995; *Hynek et al.*, 2007], Sabae and Arabia Terrae show similar valley network densities and topographic variability. These two regions cover a

large area of Mars (50° of longitude and 40° of latitude) and are thus representative of other portions of the Martian highlands where valley networks are mapped. While small diameter crater populations (<7 km) suggest that there may have been some regional variations in the processes related to crater modification, larger diameter craters (>7 km) suggest that the processes that governed valley network development ceased simultaneously. Our results suggest that valley network formation were controlled by global climatic conditions on early Mars, as opposed to more regional or local, such as sequestered volatiles released from impact cratering. This hypothesis could be confirmed by continued studies of valley network basins and subbasins as well as other highland geologic features. It is important to note that our observations do not rule out the possibility that localized valley network development occurred later in Martian history as suggested for by *Mangold* [2011] on fresh impact ejecta.

4.2. Basin Age-Dating Method

The basin crater counting technique we employed in this study provides an alternative way of constraining the timing of fluvial activity on Mars. However, it requires an extra step in determining the location of the drainage divides, and it takes longer to apply because of the larger number of craters to count. But this technique does provide a more reliable maximum age estimate because of the larger crater sampling and counting area. Having a large crater sampling also reduces the uncertainties and may explain the convergence of basin age around one value. The large age variability found by *Fassett and Head* [2008] can be explain by the fact that authors counted only craters >2 km in diameter with the buffer technique. Our sampling (average of 234 craters in each of the 27 basins or subbasins) is 8.6 times larger than *Fassett and Head* [2008] (28 in each of the 26 valley networks). *Hoke and Hynek* [2009] also found a large age variability because they used a smaller sampling of craters >1 km in diameter (mean of 157 craters in each of the five valley networks).

We observed that the age variability in the different basins is very small (<70 Myr) and is difficult to identify. Obviously, the basin technique for age-dating valley networks has limits as well. There may be some relation to N(1) ages as a function of the elevation, which may suggest that crater modification ceased at higher elevations before lower elevations [*Craddock and Maxwell*, 1993], but this hypothesis will need to be explored in a more global study.

5. Conclusions

We age-dated valley network basins and subbasins within Sabae and Arabia Terrae. Our results show (1) fluvial activity within all the basins and subbasins analyzed in this study ceased simultaneously around the Early Hesperian/Late Hesperian transition (~3.46 or 3.62 Gyr depending of the chosen Martian chronology function); (2) there is a possible correlation between degradation rate and elevation; and (3) the basin technique is a more statistically reliable technique age-dating valley networks and their drainage basins. Our primary conclusion is that valley network formation ceased because of a gradual global climate change and that this change affected all regions simultaneously. Most Martian valley networks formed during the Early Hesperian and postdate Late Noachian topographic features.

References

Aharonson, O., M. T. Zuber, D. H. Rothman, N. Schorghofer, and K. X. Whipple (2002), Drainage basins and channel incision on Mars, *Proc. Nat. Acad. Sci.*, *99*, 1780–1783.

Ansan, V., and N. Mangold (2006), New observations of Warrego Valles, Mars: Evidence for precipitation and surface runoff, *Planet. Space Sci.*, *54*, 219–242.

Banerdt, W. B., and A. Vidal (2001), *Lunar and Planetary Science XXXII* [CD-ROM], Abstract #1488, Lunar and Planetary Institute, Houston.

Bouley, S., V. Ansan, N. Mangold, P. Masson, and G. Neukum (2009), Fluvial morphology of Naktong Vallis, Mars: A late activity with multiple processes, *Planet. Space Sci.*, *57*(8–9), 982–999.

Bouley, S., R. A. Craddock, N. Mangold, and V. Ansan (2010), Characterization of fluvial activity in Parana Valles using different age-dating techniques, *Icarus*, *207*(2), 686–698.

Carr, M. H. (1995), The Martian drainage system and the origin of networks and fretted channels, *J. Geophys. Res.*, *100*, 7479–7507, doi:10.1029/95JE00260.

Carr, M. H. (1996), *Water on Mars*, 229 pp., Oxford Univ. Press, New York.

Christensen, P. R., et al. (2003), Morphology and composition of the surface of Mars: Mars Odyssey THEMIS results, *Science*, *300*(5628), 2056–2061.

Craddock, R. A., and A. D. Howard (2002), The case for rainfall on a warm, wet early Mars, *J. Geophys. Res.*, *107*(E11), 5111, doi:10.1029/2001JE001505.

Craddock, R. A., and T. A. Maxwell (1993), Geomorphic evolution of the Martian highlands through ancient fluvial processes, *J. Geophys. Res.*, *98*, 3453–3468, doi:10.1029/92JE02508.

Fassett, C. I., and J. W. Head III (2008), The timing of Martian valley network activity: Constraints from buffered crater counting, *Icarus*, *195*, 61–89.

Greeley, R., and J. J. Guest (1987), Geologic map of the eastern equatorial region of Mars, Maps 1:15,000,000, USGS Maps I-1802-B.

Gulick, V. C. (2001), Origin of the valley networks on Mars: A hydrological perspective, *Geomorphology*, *37*, 241–268.

Hartmann, W. K. (2005), Martian cratering 8: Isochron refinement and the chronology of Mars, *Icarus*, *174*, 294–320.

Hartmann, W. K., and G. Neukum (2001), Cratering chronology and evolution of Mars, *Space Sci. Rev.*, *96*(1–4), 165–194.

Hoke, M. R. T., and B. M. Hynek (2009), Roaming zones of precipitation on ancient Mars as recorded in valley networks, *J. Geophys. Res.*, *114*, E08002, doi:10.1029/2008JE003247.

Hoke, M. R. T., B. M. Hynek, and G. E. Tucker (2011), Formation timescales of large Martian valley networks, *Earth Planet. Sci. Lett.*, *312*, 1–12.

Horton, R. E. (1945), Erosional development of streams and their drainage basins: Hydrologic approach to quantitative morphology, *Geol. Soc. Am. Bull.*, *56*, 275–370.

Howard, A. D. (2007), Simulating the development of Martian highland landscapes through the interaction of impact cratering, fluvial erosion, and variable hydrologic forcing, *Geomorphology*, *91*(3–4), 332–363.

Howard, A. D., J. M. Moore, and R. P. Irwin (2005), An intense terminal epoch of widespread fluvial activity on early Mars: 1. Valley network incision and associated deposits, *J. Geophys. Res.*, *110*, E12S14, doi:10.1029/2005JE002459.

Hynek B. M., M. Beach, and M. R. T. Hoke (2007), Updated global map of Martian valley networks: Implications for hydrologic processes, Second workshop on Mars valley networks, 39.

Hynek, B. M., M. Beach, and M. R. T. Hoke (2010), Updated global map of Martian valley networks and implications for climate and hydrologic processes, *J. Geophys. Res.*, *115*, E09008, doi:10.1029/2009JE003548.

Irwin, R. P., III, and A. D. Howard (2002), Drainage basin evolution in Noachian Terra Cimmeria, Mars, *J. Geophys. Res.*, *107*(E7), 5056, doi:10.1029/2001JE001818.

Irwin, R. P., III, T. A. Maxwell, A. D. Howard, R. A. Craddock, and D. W. Leverington (2002), A large paleolakes basin at the head of Ma'adim Vallis, Mars, *Science*, *296*, 2209–2212.

Irwin, R. P., III, A. D. Howard, R. A. Craddock, and J. M. Moore (2005), An intense terminal epoch of widespread fluvial activity on early Mars: 2. Increased runoff and paleolake development, *J. Geophys. Res.*, *110*, E12S15, doi:10.1029/2005JE002460.

Irwin, R. P., III, R. A. Craddock, A. D. Howard, and H. L. Flemming (2011), Topographic influences on development of Martian valley networks, *J. Geophys. Res.*, *116*, E02005, doi:10.1029/2010JE003620.

Irwin, R. P., III, K. L. Tanaka, and S. J. Robbins (2013), Distribution of Early, Middle, and Late Noachian cratered surfaces in the Martian highlands: Implications for resurfacing events and processes, *J. Geophys. Res. Planets*, *118*, 278–291, doi:10.1002/jgre.20053.

Ivanov, B. (2001), Mars/Moon cratering rate ratio estimates, in *Chronology and Evolution of Mars*, edited by R. Kallenbach, J. Geiss, and W. K. Hartmann, pp. 87–104, International Space Science Institute, Bern.

Leopold, L. B., M. G. Wolman, and J. P. Miller (1992), *Fluvial Processes in Geomorphology*, 522 pp., Dover Publications, New York.

Mangold, N. (2011), Fluvial landforms on fresh impact ejecta on Mars, *Planet. Space Sci.*, *62*, 69–85.

Mangold, N., C. Quantin, V. Ansan, C. Delacourt, and P. Allemand (2004), Evidence for precipitation on Mars from dendritic valleys in the Valles Marineris area, *Science*, *305*, 78–81.

Martz, L. W., and J. Garbrecht (1992), Numerical definition of drainage networks from digital elevation data, *Comput. Geosci.*, *8*, 747–761.

McEwen, A. S. (2005), The rayed crater Zunil and interpretations of small impact craters on Mars, *Icarus*, *176*(2), pp. 351–381, doi:10.1016/j.icarus.2005.02.009.

Mest, S. C., and D. A. Crown (2001), Fluvial degradation of the Circum-Hellas highlands of Mars (abstract), in *Field Trip and Workshop of the Martian Highlands and Mojave Desert Analogs*, pp. 43–44, Lunar and Planetary Institute, Houston.

Milton, D. J. (1973), Water and processes of degradation in the Martian landscape, *J. Geophys. Res.*, *78*, 4037–4047, doi:10.1029/JB078i020p04037.

Palacios-Velez, O. L., and B. Cuevas-Renaud (1986), Automated river-course, ridge and basin delineation from digital elevation data, *J. Hydrol.*, *86*, 299–314.

Quantin, C., P. Allemand, N. Mangold, G. Dromart, and C. Delacourt (2005), Fluvial and lacustrine activity on layered deposits in Melas Chasma, Valles Marineris, Mars, *J. Geophys. Res.*, *110*, E12S19, doi:10.1029/2005JE002440.

Scott, D. H., and J. M. Dohm (1992), Mars highland channels: An age reassessment, *Lunar Planet. Sci.*, *XXIII*, 1251–1252.

Scott, D. H., and K. L. Tanaka (1986), Geological map of the western equatorial region of Mars (1:15,000,000), US Geol. Surv. Scientific Investigations I-1802-A.

Shreve, R. L. (1967), Infinite topologically random channel networks, *J. Geol.*, *75*, 178–186.

Smith, D. E., W. L. Sjogren, G. L. Tyler, G. Balmino, F. G. Lemoine, and A. S. Konopliv (1999), The gravity field of Mars: Results from Mars Global Surveyor, *Science*, *286*, 94–97.

Stepinski, T. F., M. M. Marinova, P. J. McGovern, and S. M. Clifford (2002), Fractal analysis of drainage basins on Mars, *Geophys. Res. Lett.*, *29*(8), 1189, doi:10.1029/2002GL014666.

Strahler, A. N. (1952), Dynamic basis of geomorphology, *Geol. Soc. Am. Bull.*, *63*, 923–938.

Tanaka, K. L. (1982), A new time-saving crater-counting technique, with application to narrow features, *NASA Tech. Memo. 85127*, pp. 123–125, U.S. Geol. Surv., Flagstaff, Ariz.

Tanaka, K. L. (1986), The stratigraphy of Mars. Proc. Lunar Sci. Conf. 17, Part 1, *J. Geophys. Res.*, *91*(Suppl.), E139–E158, doi:10.1029/JB091iB13p0E139.

Tanaka, K. L., J. A. Skinner, and T. M. Hare (2005), Geological map of the Northern Plains of Mars (1:15,000,000), USGS. [Available at http://pubs.usgs.gov/sim/2005/2888/.]

Tarboton, D. G. (1997), A new method for the determination of flow directions and upslope areas in gridded digital elevation models, *Water Resour. Res.*, *33*, 309–319, doi:10.1029/96WR03137.

Werner, S. C., and K. L. Tanaka (2011), Redefinition of the crater-density and absolute-age boundaries for the chronostratigraphic system on Mars, *Icarus*, *215*, 603–607.

Zhang, W., and D. R. Montgomery (1994), Digital elevation model grid size, landscape representation, and hydrologic simulations, *Water Resour. Res.*, *30*, 1019–1028, doi:10.1029/93WR03553.